ADVANCED FUNCTIONAL MATERIALS
www.afm-journal.de

Integration of 2D and 3D Thin Film Glassy Carbon Electrode Arrays for Electrochemical Dopamine Sensing in Flexible Neuroelectronic Implants

Jules J. VanDersarl, André Mercanzini, and Philippe Renaud**

Here we present the development and characterization of a flexible implantable neural probe with glassy carbon electrode arrays. The use of carbon electrodes allows for these devices to be used as chemical sensors, in addition to their typical use as electrical sensors and stimulators. The devices are fabricated out of polyimide, platinum, titanium, and carbon with standard microfabrication techniques on carrier wafers. The devices are released from the substrate through either chemical or electrochemical dissolution of the underlying substrate material. The glassy carbon electrode arrays are produced through the pyrolysis of SU-8 pillars at 900 °C as the first process step, as this temperature is incompatible with the other device materials. The process demonstrated here is generally applicable, allowing for the integration of various high temperature materials into flexible devices.

1. Introduction

Electrical stimulation of neuronal cells has been shown to be an effective treatment for disorders such as Parkinson's, epilepsy, depression, and obesity.[1,2] Electrode implants are also an essential part of many prosthetic devices and therapeutic regimens,[3] such as retinal[4] or auditory prosthesis,[5] limb movement restoration,[6] and brain-machine interfaces.[7,8] Traditionally, these implant electrodes were large and symmetric, stimulating a correspondingly large and ill-defined tissue volume. However, recent trends in device design have focused on smaller and directional electrodes, which stimulate a more precise tissue volume, increasing treatment efficacy and minimizing side effects.[9]

In addition to the growing use of microelectrodes, many researchers are also developing flexible implants.[8] Traditional 'stiff' devices produce a strong tissue reaction to the implant, resulting in the electrodes being encapsulated by fibrous tissue. This has the effect of electrically isolating the implant from the target tissue, which reduces implant efficacy.[1] Some of the tissue reaction is caused by the trauma of device insertion, but recent studies have shown that flexible implants result in a smaller tissue reaction,[10] and thus better protect implant functionality. This positive result is due to a flexible implant better matching the brain tissue modulus. Better modulus matching helps avoid chronic irritation at the implant-tissue interface. Flexible implants can be more difficult to implant, however, and a variety of techniques are in development to easy implantation, including implantation guides, securing the shaft of the implant to a stiff support (so that only the very tip is actually flexible), and bioresorbable coatings that temporary stiffen the device for implantation, but dissolve away in vivo.[11,12] The use of drug-eluting implant coatings is also used as a means to limit tissue reaction.[13]

Implants provide treatment by supplying an electric pulse sequence to the surrounding tissue. This has the effect of creating local area electric field gradients, which depolarize cellular membranes and trigger action potentials.[14] However, the exact mechanism under which stimulation improves patient outcome is still under debate. Although the effectiveness of a treatment protocol is ultimately determined by patient symptom improvement, more precise information about the biological effects of a stimulation series can be observed by monitoring the synaptic signaling response of surrounding neurons. Synaptic signaling can be detected with electrical sensing at the implanted electrodes. Although the ideal physical characteristics of stimulation and sensing electrodes differ,[2] a single implant that both stimulates and monitors electrical response to treatment is possible.[15] However, electrical signal changes are often difficult to translate into meaningful diagnostic information. In contrast, information about changes in brain chemistry has been carefully researched and is of great interest to the medical community. In fact, most medication targeting DBS (deep brain stimulation) treatable diseases works by altering the chemical balance in the brain tissue. Fortunately, techniques have also been developed recently to use electrodes to monitor chemical levels in vivo with electrochemical sensing.[16,17] This means that with a single implanted electrode device it is possible to provide therapeutic stimulation and monitor the treatment's effects through both chemical and electrical changes.

J. J. VanDersarl, P. Renaud
Microsystems Laboratory, EPFL-STI-IMT-LMIS4
École Polytechnique Fédérale de Lausanne (EPFL)
1015, Lausanne, Switzerland
E-mail: julesvan@gmail.com; philippe.renaud@epfl.ch
A. Mercanzini
Aleva Neurotherapeutics SA
EPFL Innovation Park D
1015, Lausanne, Switzerland

DOI: 10.1002/adfm.201402934

Although all implanted electrodes must be stable and biocompatible, the material and design requirements can vary widely depending on their application. Stimulating electrodes need to inject a certain amount of charge, and thus need to be relatively large or use a material with a high charge injection density,[2] while electrical sensing electrodes require low impedance to limit noise.[2] Chemical sensing electrodes detect different chemicals by oxidizing (or reducing) them at the electrode surface. This requires an electrode material that can stably reach the necessary voltages to oxidize the target chemical (a wide 'water window'), and one that will not be fouled following species oxidation. Additionally, the efficiency/specificity of chemical sensing electrodes can be strongly affected by the electrode surface groups.

Currently, carbon is the most popular material for chemical sensing electrodes. The oxidation/reduction of chemicals at an electrode surface occur at a specific voltage, and carbon electrodes can operate in water environments over a wider range of voltages than other electrode materials, such as platinum,[18] which allows for detection of a wider range of analytes. For example, high speed cyclic voltammetry can reduce and oxidize the neurotransmitter dopamine in distinct peak patterns within the carbon water window, but these peaks occur outside of the platinum water window.[18]

Carbon electrodes can be deposited through screen or inkjet printing, but these electrodes are comprised of microscopic stacks of graphite sheets packed against each other after solvent evaporation. The final structure relies on a percolated network of these individual structures to pass charge, and is much less electrical and mechanically stable than a continuous structure, as percolated network resistance is dominated by a few single 'hops' between units with high energy barrier,[19,20] and these films typically have inferior electrochemical properties to carbon fiber electrodes.[21] Glassy (vitrous) carbon does not have these problems. The structure is a single unit, comprised or a continuous ribbon-like structure of sp2 carbon.[22] This type of carbon is chemically inert, non-adhesive, and is well regarded in the electrochemistry community for is stability. By pyrolyzing lithographically defined photoresists, scientists can easily create micrometer scale glassy carbon electrodes on wafers massively in parallel and with great precision.[23] This technique has already been used to make glassy carbon electrodes on stiff, silicon based neural implants.[21]

Previous researchers have developed processes for creating flexible neural implants on carrier wafers using standard semiconductor technology, and have successfully transferred the technical process to industry. This fabrication process involved depositing platinum electrodes between two layers of polyimide and etching the devices to the appropriate shape.[24] The devices were then released by electrochemically dissolving an aluminum thin film between the devices and the carrier wafer.[25] However, neither the aluminum underlayer nor the polyimide can survive the high temperature pyrolysis process (900 °C) used to generate the glassy carbon electrodes, so a new device release techniques and process flow needed to be developed.

2. Design and Fabrication

Through the use of new materials and procedures we have successfully fabricated flexible neural implants with glassy carbon electrodes. The implants are fabricated out of well-established biocompatible materials; polyimide, titanium, platinum, and glassy carbon. The implant arms can be bent to a 1mm radius without altering device performance due to the glassy carbon being confined to the electrode tip, and the internal platinum wiring being located at the neutral axis of the implant shaft (**Figure 1**A). A variety of electrode sizes and designs are achievable using pyrolysis of photo-definable resist patterns, including patterns for DBS (Figure 1C) or retinal prosthesis (Figure 1D) applications. The DBS electrodes are large, comprised of a 5 × 5 array of 200 µm × 200 µm square electrodes, spaced 50 µm apart, wired together to effectively create single 1 mm^2 surface area electrodes. The retinal implant design is inspired by previous work,[26] and consists of 30 µm diameter electrodes spaced 200 µm apart in a 3 × 3 electrode array, which is circumscribed by a counter electrode ring.

The high temperatures needed to pyrolyze photoresist into glassy carbon also destroy polyimide. Therefore, the electrodes need to be made first, and the rest of the neural probes are then built around them. Although this paper describes the example of glassy carbon electrodes, this process has application for the integration of any electrode materials that is brittle and/or uses high temperature processing (such as chemical vapor deposition (CVD) deposited diamond[27]) onto a flexible backbone.

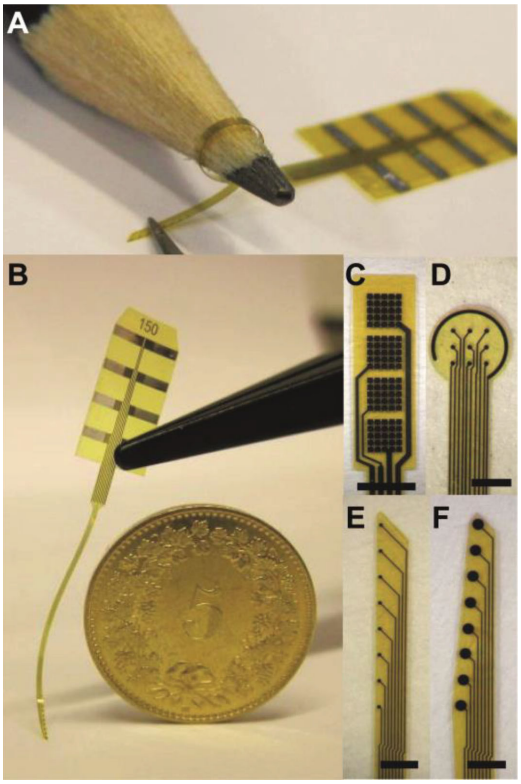

Figure 1. A) Implant probes shafts are very flexible, and B) return to their original shape after flexing (the Swiss 5-cent piece is ≈17 mm in diameter). C) Electrodes designed for DBS (5 × 5 arrays of 200 × 200 µm square electrodes, spacing 50 µm), D) retinal stimulation (3 × 3 array of 30 µm electrodes, spacing 200 µm), or E) linear arrays with 50 µm (spacing 400 µm) or F) 150 µm (spacing 400 µm) electrodes. Scale bars: C:2000µm, D:800 µm, E:500 µm, F:500 µm

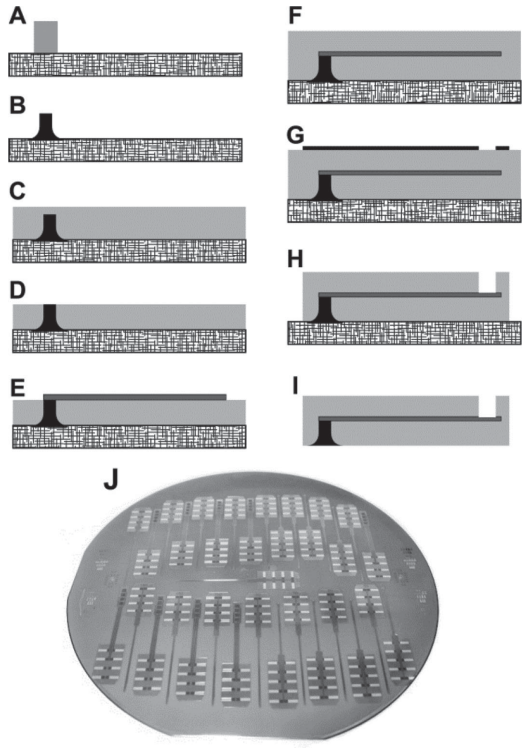

Figure 2. The basic process flow includes A) defining the photoresist electrode patterns, B) pyrolyzing the resist into electrodes, C) depositing a layer of polyimide, D) exposing the electrodes via polyimide CMP, E) depositing and defining Ti/Pt/Ti metallic lines to the electrodes, F) a second layer of polyimide, G) deposition and patterning of a SiO_2 film, H) plasma etching of the polyimide to the define the final implant shape, and I) release of the implants from the substrate. J) The devices are entirely processed on a 100mm carrier wafer.

The process flow used to create the flexible implants with glassy carbon electrodes is shown in **Figure 2** and described in detail in the methods section. In brief, the glassy carbon electrodes are created from pillars of photolithographically defined SU-8 photoresist, which are then pyrolized under nitrogen at 900 °C. Polyimide is then spun and cured over the electrodes, and then access to the electrode backsides is created via CMP (chemical-mechanical polishing) of the polyimide. The metallic wiring of the implant is then deposited and defined via sputtering and photolithography. Next, a second layer of polyimide is spun and cured and then coated with a PVD (physical vapor deposition) SiO_2 thin film. Finally, the device structure is defined lithographically, and dry etched to shape. Most of this process is easily understood, but several steps have important features or innovations and are detailed below.

In order to ensure a mechanically robust implant, the glassy carbon electrodes need to be strongly bound to the surrounding polyimide. However, glassy carbon is notorious for being resistant to reactions and binding, evident by its popularity for evaporator crucibles. Glassy carbon is ribbon like in structure, and has surface functionalities of both hydroxyl and carbonyl groups[28] which are increased in surface density through surface treatments including KOH,[28] HNO_3,[28] and oxygen plasma.[29] In Figure 2C, we first expose the glassy carbon electrodes to 60s 500W oxygen plasma to increase the density of oxygen surface groups. These surface groups are then used to covalently[30] bind proprietary (3-aminopropyl)triethoxysilane (APTES) functionalities (VM651, HD Microsystems, Cupertino, CA, USA), which in turn incorporate into the polyimide layers. This ensures a robust bond between the glassy carbon electrodes and the polyimide device backbone, as confirmed by peel tests.

DBS treatments often require a large amount of charge transfer, which necessitates large surface area electrodes, typically 1000 μm × 1000 μm. Fabricating single glassy carbon electrodes with these dimensions has a low yield, however. During pyrolysis the photoresist can volumetrically contract as much as 90%.[22] Because the SU-8 structures are constrained by their wafer footprint, this contraction creates a great deal of interfacial strain at the carbon-wafer interface. For a given footprint area, there is a maximum height that the photoresist can be before the stress from pyrolysis causes the electrode to delaminate from the surface. This results in a 1000 μm × 1000 μm glassy carbon electrode having a maximum height of approximately 5 μm. This creates large electrodes with a relatively small electrode-polyimide interface, which should be maximized for a robust device.

In order to increase the robustness of implants with large area electrodes, the electrodes are broken into arrays of smaller electrodes, which are then wired together to act as a single electrode. The large DBS electrodes are replaced with a 5 × 5 electrode array with the same total area (Figure 1C). This results in a 5× increase in total electrode circumference, and a 4× increase in electrode height (since electrodes with a smaller footprint can be made taller,[21] resulting in a 20× increase in electrode-polyimide contact area. Stimulation theory says that the electrode array will not have any adverse effects on the device efficacy.[31] In fact, smaller electrodes can have a higher specific current density than larger electrodes,[2] so a same area multi-electrode array could potentially improve performance over a single large electrode.

In addition to the interface between the glassy carbon electrodes and the polyimide, the electrical interface between the electrodes and the metal wiring is also of critical importance. Previously, an oxygen plasma treatment followed by a PVD titanium deposition had been demonstrated to create a robust mechanical and thermal-electrical bond between glassy carbon and metals.[32] Using 60 s 500 W in vacuo oxygen plasma before rf sputtered titanium deposition produces a good electrical interface between the carbon electrodes and the platinum wiring, as is demonstrated by impedance measurements (**Figure 3**).

To release the implant devices from the carrier wafer, dissolving a sacrificial film under the devices is typically used. The use of selective chemical etching is possible, but since lateral etching is diffusion rate limited,[25] releasing the devices can take days. Over such long etch times, even very selective chemical etchants can begin to attack other materials.[33] Anodic dissolution of the sacrificial layer occurs at accelerated rates compared to the diffusion limited chemical etching, thus, finding a replacement for aluminum as a sacrificial layer is desirable.[25]

Metals that easy oxidize in salt water environments, such as aluminum, zinc, and cadmium, tend to have melting temperatures below the pyrolysis temperature. Some of these materials

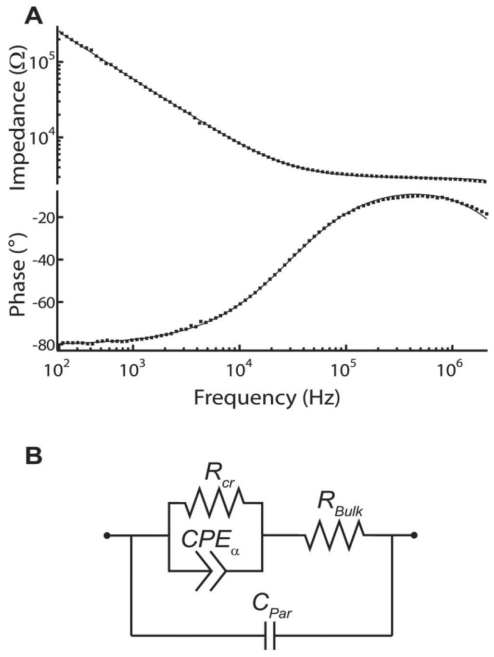

Figure 3. A) Bode plots show the impedance and phase behavior of 150 µm diameter glassy carbon electrodes at ±100 mV in 1xPBS (conductivity 1.6×10^{-2} S cm^{-1}). B) The circuit model for electrode behavior.

also introduce additional problems by oxidizing to non-soluble solids or being non-standard clean room materials. Another easily oxidizable metal, iron, forms deep level traps, and is therefore unwelcome in most cleanroom machines. Tungsten is an obvious target for a high temperature processing, as it has the highest melting point of all pure metals. Furthermore, it is considered an active anodic material in saline solutions, although less so than the metals mentioned above.

The use of tungsten as the sacrificial layer does come with issues, however. Tungsten develops a self-passivating oxide that protects against dissolution at neutral pHs.[34] Thus, tungsten dissolution needs to be done in a basic solution, which can dissolve the tungsten oxide.[35] However, basic pHs can affect the neural probe materials over long times.[33] Additionally, although metals like tungsten are able to easily resist melting pyrolysis temperatures, carbide or nitride formation can occur, which are difficult to remove. To prevent tungsten carbide or nitride formation, the tungsten film is coated with a 250 nm SiO_2 passivation layer (Figure S1a).

Because tungsten dissolution needs to occur in a basic solution, minimizing the time it takes the implants to be released is important. Applying an AC voltage signal, rather than DC, can dramatically increase the tungsten dissolution rate,[36] which limits device exposure time to the base solution, and results in the devices being released even faster than with aluminum sacrificial films. Additionally, hydroxide etch rates are highly dependent on temperature,[37] and are nearly negligible at room temperature, where we perform anodic dissolution. For additional protection, various protective resists specifically designed to protect sensitive structures from basic solutions can be coated onto the devices.[38] The devices shown in Figures 1B, 1D, and 1E were successfully released using these methods, and without protective resists.

For structures or devices with a low tolerance for exposure to base solutions, dissolving the carrier wafer proved to be a successful release process. Starting with a silicon wafer with a thermal oxide, the devices were made as before, and the entire top surface of the wafer was coated with KOH resistant resist (ProTek B3 resist, Brewer Science, USA) (Figure S2). The wafer backside was then ground until the entire wafer was 150 µm thick, and then the remaining silicon was dissolved in a bath of 10% KOH at 40 °C. The resultant structure was a sheet of probes sandwiched between the protective resist and a SiO_2 film. A 30min soak in acetone dissolves the resist, and a 2min dip in 2% hydrofluoric acid removes the SiO_2. The devices shown in Figures 1A, 1C, and 1F were released using this method.

3. Device Testing

Fabricating the implants using semiconductor processes allows us to leverage this mature technology to create massively parallel processed probes with very high precision. These designs are based on electrode arrays, so consistent performance between electrodes is important. These electrodes, for example, can be used for large area chemical mapping of large areas or act as controls against each other, both of which rely of high electrode repeatability.

Electrode characterization of the devices in PBS demonstrates that the electrochemical properties of the devices are consistent with carbon electrodes (Figure 3). These results show a successful electrical contact between the glassy carbon electrodes and the sputtered titanium adhesion layer.

Electrochemical impedance spectroscopy is a useful tool to understand the properties of an electrode.[39,40] Using these results an equivalent circuit for the electrode can be determined, which clearly illustrates device properties. A typical implanted electrode circuit is comprised of model circuits for the microelectrode surface, the bulk tissue resistance (R_{Bulk}), and stray wiring capacitance (C_{par}). The microelectrode interface can be modeled by resistor (charge transfer resistance, R_{cr}) and a constant phase element (double layer capacitance, CPE_α) in parallel.[1] The complete circuit is shown in Figure 3b.

Fitting the equivalent circuit model (Figure 3b) to empirical data (Figure 3a, black dots) with the program ZView (Scribner Associates, Inc, Southern Pines, NC) produces an excellent fit ($\chi^2 < 0.001$). The data was taken using a 100 mV AC signal from 10^2–10^6 Hz in 1× PBS at 20 °C. The fit (Figure 3a, black line) generates values of R_{Bulk} = 3000 Ω (for a buffer conductivity of 0.5 Ω cm) and CPE_T = 12 nF (70 µF cm^{-2}). These values are as expected for glassy carbon electrodes of this size in saline.[1,41–44] For electrochemical impedance spectroscopy in the absence of an electroactive species, R_{cr} is considered infinite, which demonstrates the lack of Faradaic current with these electrodes; virtually all the change transfer is capacitive, which is the preferred mechanism for implanted electrodes. The parasitic capacitance, C_{Par}, is approximately 1.9pF, which is a good value for this type of polyimide implant.[1]

As a characterization of the electrochemical behavior of the electrodes, as well as a demonstration of their consistent

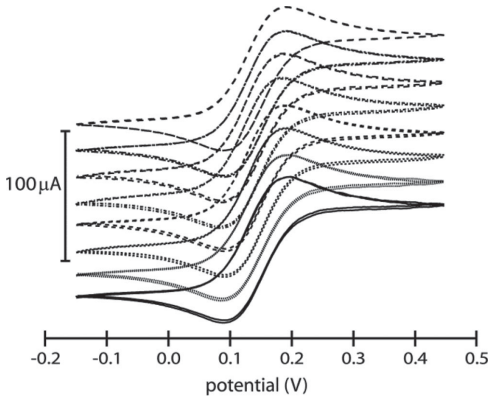

Figure 4. Cyclic voltammetry sweeps in 2 mM FeMeOH and 0.1 M KCl at 50 mV s^{-1} with a 150 μm, 8 electrode implant. All sweeps were done concurrently. The curves are offset vertically by 20 μA for visual clarity.

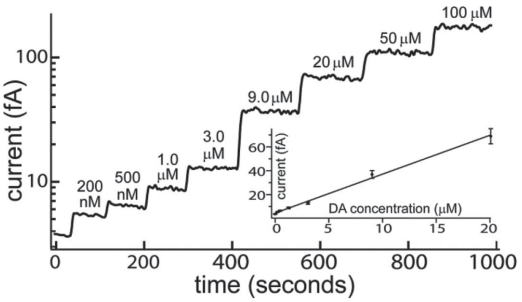

Figure 5. Amperometric detection of dopamine in PBS with 150 μm electrodes at +500 mV with an Ag/AgCl counter electrode and reference electrode. The relationship between current and concentration is linear up to 20 μM with an r^2 of 0.996 (insert).

performance relative to each other, we tested the implants using cyclic voltammetry in a solution of 2 mM FeMeOH in 0.1 M KCl filtered through a 0.2 μm syringe filter. Each 150 μm electrode performed identically over multiple cycles – the electrochemical curves are offset in **Figure 4** for visual clarity. The electrodes were all tested at the same time, which demonstrates that the electrodes and wiring lines are well insulated electrically from each other, with no leaks between electrode pairs. This also acts as a basic in vitro proof of concept for simultaneous chemical detection across many electrodes, with applications for either area mapping or multiple electrode systems.

Many biochemicals can be detected through electrochemical techniques, including dopamine, serotonin, norepinephrine, and DOPAC.[18] Among these, dopamine is perhaps of greatest interest, due to its prevalence in motor control, motivation, and reinforcement learning.[45] Dopamine concentration changes are also scientifically interesting over both sub-second and chronic timescales. Electrical stimulation, light stimulation, wound healing, and mood have all been related to dopamine levels in the brain. Because of this, there is great interest in monitoring dopamine levels in vivo.

Dopamine levels can be detected electrochemically with carbon electrodes using either amperometry or cyclic voltammetry. When sufficient potential is applied to an electrode, dopamine donates two electrons and is oxidized to dopamine-o-quinone, producing a current. During cyclic voltammetry, at the return potential dopamine-*o*-quinone will accept two electrons and reduce back to dopamine.[17] Amperometry can detect concentration changes very fast and is simple, requiring little processing power or data post processing.[16] Cyclic voltammetry, especially fast scan cyclic voltammetry (>400 V/s), is of increasing interest for in vivo measurements, as oxidation peaks from different molecules can be deconvolved to provide more molecule specific concentration data.[18,21] However, this technique comes with a cost of increased data processing requirements and slower temporal resolution. As a proof of concept, we tested our devices with in vitro amperometric detection of titrated dopamine in a solution of phosphate buffered saline.

The results of a dopamine titration with the electrodes from Figure 1d are shown in **Figure 5**. Amperometric detection is done at +500 mV, below the peak oxidation potential of dopamine, +600 mV vs Ag/AgCl.[18] Dopamine detection shows a linear response (r^2 >0.99) up to 20 μM before losing linearity, which equals or exceeds the linear detection range of others.[15,21] The limit of detection, defined as 3 times the signal standard deviation above the blank, is approximately 65 nM. This detection limit is similar to the findings of others.[21]

4. 3D Electrodes

As the wafer surface acts as a mold for the glassy carbon electrodes, the electrode shape can be altered by editing the wafer accordingly. Flat, circular electrodes are easy to manufacture and are simple to understand and simulate due to their symmetrical electrical fields. Different electrode shapes and 3D electrodes produce more complicated electric fields and can locally focus electric fields at sharp features, although these local changes to the local electric field do not extend far from the electrode surface (no more than 2–3× the diameter of the electrode).[46] Despite this, local electric field focusing can be of value, and 3D electrodes can extend away from the implanted electrode, beyond tissue encapsulation, and closer to live, active neurons. This technique is currently in wide use for in vitro MEAs (micro electrode arrays) to interrogate brain slices ex vivo.[47] In a similar way, we can use pyramidal glassy carbon electrodes to extend the electrode away from the flexible implant bodies.

Creating pyramidal pits in a wafer is a well understood microfabrication process, and does not add any masks to the process, although it does add a lithography step (one mask is used twice). The altered process flow is detailed in Figure S3, and starts with a < 100 > silicon wafer to allow for pyramidal KOH etching. Devices made with 3-dimensional pyramidal electrodes are shown in **Figure 6**.

Due to the large volume change of the SU-8 during pyrolysis there is a limit as to the size of the pyramidal electrode that can be successfully created through a single pyrolysis step. The largest sized pyramids we reliably producible with a single pyrolysis are approximately 150 μm. Larger pyramids result in void formation or delamination from the mold surface. However, serial pyrolysis, where relatively thin amounts of SU-8 are defined, pyrolized, and then more resist is deposited and pyrolized, can overcome this size barrier.

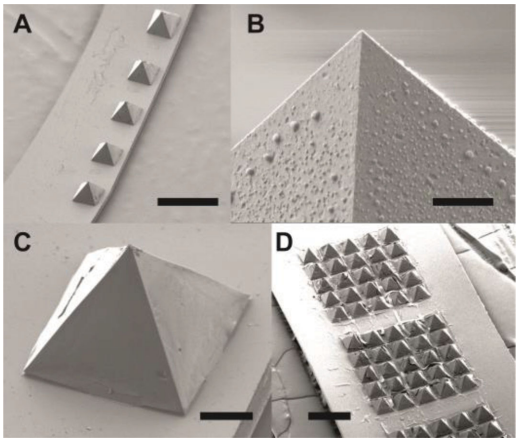

Figure 6. Pyramidal electrodes of various sizes and array types. Scale bars: A:300 μm, B:2 μm, C:50 μm, D:500 μm.

5. Conclusions

In conclusion, we have demonstrated a new process for integrating high temperature materials into flexible substrates. This was demonstrated with flexible polyimide neuron probe implants and glassy carbon electrodes. Such devices are highly relevant for long term chemical monitoring in vivo. The processes shown here are also generally relevant to other high temperature and non-compatible materials, such as high temperature CVD deposited materials. We also demonstrated two systems to release high temperature devices from the carrier wafer, as well as the fabrication and integration of 3-dimensional electrodes.

Supporting Information

Supporting Information is available from the Wiley Online Library or from the author.

Acknowledgments

The authors thank the staff at the EPFL Center for Micronanotechnology (CMi) for their support and advice during device fabrication, especially Cyrille Hibert, Didier Bouvet, Anthony Guillet, and Laszlo Petho. Pyrolysis was done in the Laboratory of Microengineering for Manufacturing at EPFL under Prof. Peter Ryser, with support from Gael Farine. Additional technical expertise on photoresist pyrolysis was provided by Dr. Rodrigo Martinez-Duarte of LMIS4 at EPFL. Electrochemical measurements were performed in the Laboratory of Physical and Analytical Electrochemistry (LEPA) at EPFL run by Prof. Hubert Girault, with assistance from Dr. Andreas Lesch and Dr. Fernando Cortes Salazar. Preliminary work on the project was done by Lynda Metref and Ludovica Colella of LMIS4 at EPFL. The authors thank Farnoosh Vahidpour and Milos Nesladek from IMEC for useful discussions. The authors acknowledge the financial support of the Swiss Innovation Promotion Agency (CTI), project 10746.1 PFNM-NM.

Received: August 26, 2014
Published online: November 6, 2014

[1] A. Mercanzini, P. Colin, J.-C. Bensadoun, A. Bertsch, P Renaud, *IEEE Trans. Biomed. Eng.* **2009**, *56*, 1909.
[2] S. F. Cogan, *Ann. Rev. Biomed. Eng.* **2008**, *10*, 275.
[3] L. R. Hochberg, M. D. Serruya, G. M. Friehs, J. A. Mukand, M. Saleh, A. H. Caplan, A. Branner, D. Chen, R. D. Penn, J. P. Donoghue, *Nature* **2006**, *442*, 164.
[4] M. S. Humayun, J. D. Weiland, G. Y. Fujii, R. Greenberg, R. Williamson, J. Little, B. Mech, V. Cimmarusti, G. Van Boemel, G. Dagnelie, *Vision Res* **2003**, *43*, 2573.
[5] L. M. Friesen, R. V. Shannon, D. Baskent, X Wang, *J. Acoustical Soc. Am.* **2001**, *110*, 1150.
[6] R Van den Brand, J. Heutschi, Q. Barraud, J. DiGiovanna, K. Bartholdi, M. Huerlimann, L. Friedli, I. Vollenweider, E. M. Moraud, S. Duis, N. Dominici, S. Micera, P. Musienko, G. Courtine, *Science* **2012**, *336*, 1182.
[7] M. Jenkner, B. Müller, P. Fromherz, *Biol. Cybernet.* **2001**, *84*, 239.
[8] X. Navarro, T. B. Krueger, N. Lago, S. Micera, T. Stieglitz, P. Dario, *J. Periph. Nervous Syst.* **2005**, *10*, 229.
[9] C. Pollo, A. Kaelin-Lang, M. F. Oertel, L. Stieglitz, E. Taub, P. Fuhr, A. M. Lozano, A. Raabe, M. Schuepbach, *Brain* **2014**, DOI: 10.1093/brain/awu102.
[10] A. Mercanzini, K. Cheung, D. Buhl, M. Boers, A. Maillard, P. Colin, J.-C. Bensadoun, A. Bertsch, A. Carleton, P. Renaud, *IEEE 20th Int. Conf. Micro Electro Mechanical Systems* **2007**, 573.
[11] T. Suzuki, K. Mabuchi, S. Takeuchi, *First Int. IEEE EMBS Conf. Neural Engineering* **2003**, 154.
[12] L. W. Tien, F. Wan, M. D. Tang-Schomer, E. Yoon, F. G. Omenetto, D. L. Kaplan, *Adv. Funct. Mater.* **2013**, *23*, 3185.
[13] A. Mercanzini, S. T. Reddy, D. Velluto, P. Colin, A. Maillard, J.-C. Bensadoun, J. A. Hubbell, P. Renaud, *J. Controlled Release* **2010**, *145*, 196.
[14] A. K. Ahuja, M. R. Behrend, M. Kuroda, M. S. Humayun, J. D. Weiland, *IEEE Trans. Biomed. Eng.* **2008**, *55*, 1744.
[15] M. D. Johnson, R. K. Franklin, M. D. Gibson, R. B. Brown, D. R. Kipke, *J. Neurosci. Methods* **2008**, *174*, 62.
[16] K. T. Kawagoe, R. M. Wightman, *Talanta* **1994**, *41*, 865.
[17] P. E. Phillips, R. M. Wightman, *TrAC Trends Anal. Chem.* **2003**, *22*, 509.
[18] D. L. Robinson, B. J. Venton, M. L. Heien, R. M. Wightman, *Clin. Chem.* **2003**, *49*, 1763.
[19] D. Stauffer, A. Aharony, *Introduction to Percolation Theory*, Taylor and Francis, London, **1994**.
[20] P. A. Lee, *Phys. Rev. Lett.* **1984**, *53*, 2042.
[21] M. K. Zachek, P. Takmakov, B. Moody, R. M. Wightman, G. S. McCarty, *Anal. Chem.* **2009**, *81*, 6258.
[22] R. Martinez-Duarte, G. T. Teixidor, P. P. Mukherjee, Q. Kang, M. J. Madou, in *Microfluidics and Microfabrication*, **2010**, Springer, New York, 181.
[23] R. Martinez-Duarte, P. Renaud, M. J Madou, *Electrophoresis* **2011**, *32*, 2385.
[24] A. Mercanzini, K. Cheung, D. L. Buhl, M. Boers, A. Maillard, P. Colin, J.-C. Bensadoun, A. Bertsch, P. Renaud, *Sens. Actuat. A: Phys.* **2008**, *143*, 90.
[25] S. Metz, A. Bertsch, P Renaud, *J. Microelectromech. Syst.* **2005**, *14*, 383.
[26] J. Salzmann, O. P. Linderholm, J.-L. Guyomard, M. Paques, M. Simonutti, M. Lecchi, J. Sommerhalder, E. Dubus, M. Pelizzone, D. Bertrand, J. Sahel, P. Renaud, A. B. Safran, S. Picaud, *Br. J. Ophthalmol.* **2006**, *90*, 1183.
[27] S. Koizumi, C. Nebel, M. Nesladek, *Physics and Applications of CVD Diamond*, Wiley-VCH, Weinheim, **2008**.
[28] K. G. Ray, R. L. McCreery, *J. Electroanal. Chem.* **1999**, *469*, 150.
[29] A. Paproth, K.-J. Wolter, R. Deltschew, in *Proc. 56th Electronic Components and Technology Conference* **2006**, 959.
[30] J. Liu, L. Cheng, B. Liu, S. Dong, *Langmuir* **2000**, *16*, 7471.
[31] O. G. Martinsen, S. Grimnes, *Bioimpedance and Bioelectricity Basics*, Academic Press, London, **2008**.

[32] E. Neubauer, G. Korb, C. Eisenmenger-Sittner, H. Bangert, S. Chotikaprakhan, D. Dietzel, A. M. Mansanares, B. K. Bein, *Thin Solid Films* **2003**, *433*, 160.
[33] K. R. Williams, K. Gupta, M. Wasilik, *J. Microelectromech. Syst.* **2003**, *12*, 761.
[34] J. W. Johnson, C. L. Wu, *J. Electrochem. Soc.* **1971**, *118*, 1909.
[35] R. D. Armstrong, K. Edmondson, R. E. Firman, *J. Electroanal. Chem. Interfacial Electrochem.* **1972**, *40*, 19.
[36] A. D. Davydov, V. S. Shaldaev, A. N. Malofeeva, I. V. Savotin, *J. Appl. Electrochem.* **1997**, *27*, 351.
[37] H. Tanaka, S. Yamashita, Y. Abe, M. Shikida, K Sato, *Sens. Actuat. A: Phys.* **2004**, *114*, 516.
[38] R. A. Rahim, B. Bais, B. Y. Majlis, G Sugandi, in *Symp. Design, Test, Integration and Packaging of MEMS/MOEMS (DTIP)* **2012**, 204.
[39] E. T. McAdams, A. Lackermeier, J. A. McLaughlin, D. Macken, J Jossinet, *Biosensors and Bioelectronics* **1995**, *10*, 67.
[40] A. S. Bandarenka, *Analyst* **2013**, *138*, 5540.
[41] T. Shigemitsu, G. Matsumoto, S. Tsukahara, *Med. Biol. Eng. Comput.* **1979**, *17*, 465.
[42] A. S. Sarac, M. Ates, B. Kilic, *Int. J. Electrochem. Sci* **2008**, *3*, 777.
[43] P. Heiduschka, A. W. Munz, W. Göpel, *Electrochim. Acta* **1994**, *39*, 2207.
[44] G. M. Swain, *J. Electrochem. Soc.* **1994**, *141*, 3382.
[45] J. J. Clark, S. G. Sandberg, M. J. Wanat, J. O. Gan, E. A. Horne, A. S. Hart, C. A. Akers, J. G. Parker, I. Willuhn, V. Martinez, *Nat. Methods* **2010**, *7*, 126.
[46] H. Kasi, W. Hasenkamp, G. Cosendai, A. Bertsch, P. Renaud, *J. Neuroeng. Rehabil* **2011**, *8*, 44.
[47] M. O. Heuschkel, M. Fejtl, M. Raggenbass, D. Bertrand, P. Renaud, *J. Neurosci. Methods* **2002**, *114*, 135.